PHYSICAL REVIEW C **67**, 041303(R) (2003)

Transition quadrupole moments in the superdeformed band of ^{40}Ca

C. J. Chiara, E. Ideguchi,* M. Devlin,† D. R. LaFosse, F. Lerma,‡ W. Reviol, S. K. Ryu, and D. G. Sarantites
Department of Chemistry, Washington University, St. Louis, Missouri 63130

C. Baktash and A. Galindo-Uribarri
Physics Division, Oak Ridge National Laboratory, Oak Ridge, Tennessee 37831-6371

M. P. Carpenter, R. V. F. Janssens, T. Lauritsen, C. J. Lister, P. Reiter, and D. Seweryniak
Physics Division, Argonne National Laboratory, Argonne, Illinois 60439-4843

P. Fallon, A. Görgen,§ and A. O. Macchiavelli
Nuclear Science Division, Lawrence Berkeley National Laboratory, Berkeley, California 94720

D. Rudolph
Department of Physics, Lund University, S-22100 Lund, Sweden

(Received 21 January 2003; published 28 April 2003)

The transition quadrupole moments Q_t for the superdeformed band in ^{40}Ca have been determined through thin-target Doppler-shift attenuation analyses. A best-fit value of $Q_t = 1.30 \pm 0.05$ *e* b is obtained when a single value is assumed for the entire band. Fitting separate quadrupole moments for in-band transitions decaying from the high-spin states and the presumably admixed low-spin states results in $Q_t(\text{high}) = 1.81^{+0.41}_{-0.26}$ *e* b and $Q_t(\text{low}) = 1.18^{+0.06}_{-0.05}$ *e* b, respectively. Q_t values extracted for individual transitions in a Doppler-broadened line-shape analysis also indicate smaller Q_t values at lower spins. These results are consistent with the interpretation of this band as an eight-particle–eight-hole superdeformed band with a significant admixture of less-collective configurations at low spins.

DOI: 10.1103/PhysRevC.67.041303 PACS number(s): 21.10.Ky, 21.10.Re, 23.20.Lv, 27.40.+z

The mass $A = 40$ region has received attention recently with the discovery of superdeformed (SD) bands in ^{40}Ca [1] and ^{36,38}Ar [2–4]. The low-spin behavior of these bands is distinctive as compared to SD bands in other mass regions, in that a considerable amount of decay intensity stays within the band, nearly down to the excited 0^+ bandhead. Another important observation is that these SD bands are linked by intense, discrete transitions to spherical or normal deformed states in the respective nuclei. In each of these nuclei, the SD structures are attributed to multiparticle-multihole (np-nh) excitations across the $N,Z = 20$ spherical shell gaps into the fp shell. Nuclei in this region offer an opportunity to explore this coexistence of noncollective (spherical) and highly collective (highly deformed) states through a variety of theoretical models, including several mean field approaches and large-scale shell model calculations.

One of the most sensitive probes of the underlying structure of the deformed bands is the transition quadrupole moment Q_t. In Ref. [1], a thin-target Doppler-shift attenuation measurement was performed for ^{40}Ca, from which a large $Q_t = 1.80^{+0.39}_{-0.29}$ *e* b value was deduced for the transitions decaying from the 16^+ through 6^+ states in the SD band, assuming a fixed Q_t throughout the sequence. This value agreed with the $B(E2)$ for the 914-keV $4^+ \rightarrow 2^+$ transition in that band which was previously reported to be 100^{+56}_{-34} W.u. [5], equivalent to $Q_t = 1.69^{+0.42}_{-0.32}$ *e* b. Cranked relativistic mean field calculations predicted an equally large Q_t value for this band, $Q_t \sim 2$ *e* b [1]. An 8p-8h configuration was assigned in Ref. [1], consistent with early shell model predictions for the 0_3^+, 2_2^+, and 4_2^+ levels of the SD band that had been previously identified [6]. In Table 3 of Ref. [6], however, the calculated amplitudes of the np-nh ($n = 0,2,4,6,8$) components of the 0_3^+ wave function are provided; these indicate that there are substantial contributions to the wave function from the $n < 8$ components. Similar results were obtained from those calculations for the 2_2^+ and 4_2^+ states. The intense decay from the SD band to a second bandlike structure, proposed in Ref. [1] to be based on a 4p-4h configuration, may be a reflection of the admixtures discussed in Ref. [6]. This situation is apparent in Fig. 1, which is a partial level scheme of ^{40}Ca showing the SD band (labeled 1) and the 4p-4h band (labeled 2). This scenario in ^{40}Ca is similar to that found in ^{38}Ar, where considerable mixing was observed between 4p-6h and 2p-4h configurations at low spin [4].

One would expect the admixture of $n < 8$ np-nh configurations to reduce the Q_t value relative to the pure 8p-8h case. In light of this, the data of Ref. [1] have been reanalyzed and

*Present address: RIKEN, The Institute of Physical and Chemical Research, Saitama 351-0198, Japan.
†Present address: LANSCE-3, MS H855, Los Alamos National Laboratory, Los Alamos, NM 87545.
‡Present address: Radiation Oncology Center, Washington University, St. Louis, MO 63110.
§Present address: DAPNIA/SPhN, CEA-Saclay, F-91191 Gif-sur-Yvette Cedex, France.

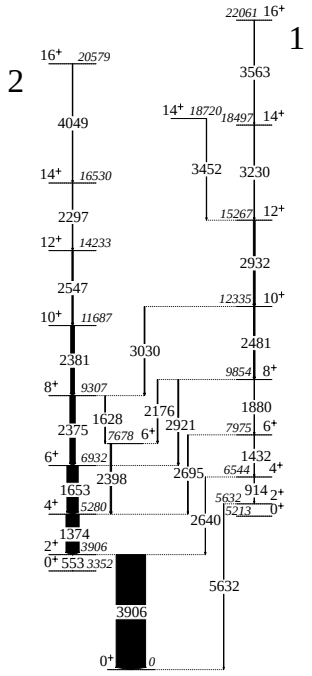

FIG. 1. Partial level scheme of ^{40}Ca showing the 8p-8h SD band 1 and the 4p-4h band 2. The arrow widths are proportional to the γ-ray intensities in the ^{28}Si(^{20}Ne,2α) reaction. Energies of states and transitions are given in keV.

combined with results from a new experiment, which include a lifetime analysis for individual states; in the current study, the Q_t moment was allowed to vary with spin to account for the possibility of changes in deformation throughout the SD band. This Rapid Communication presents the combined results from both experiments on the transition quadrupole moments in the SD band of ^{40}Ca.

Details of the first experiment, experiment 1, which populated ^{40}Ca via the ^{28}Si(^{20}Ne,2α) reaction, are provided in Ref. [1]. The second experiment produced ^{40}Ca with the reaction ^{24}Mg(^{24}Mg,2α). A 92-MeV ^{24}Mg beam was provided by the 88-Inch Cyclotron at Lawrence Berkeley National Laboratory. This reaction forms the same compound system as the previous experiment, but with a larger average initial recoil velocity $\langle\beta_0\rangle$. Two types of targets were used: a self-supporting ^{24}Mg foil of nominal thickness 0.5 mg/cm^2 (experiment 2a), and a 0.5-mg/cm^2 ^{24}Mg foil backed with 3.6-mg/cm^2 Ta (experiment 2b). Emitted γ rays were detected with the Gammasphere array [7], which consisted of 102 Compton-suppressed high-purity Ge detectors arranged in 16 rings of constant angle θ relative to the beam axis. The Microball array of 95 CsI(Tl) detectors was used for charged-particle identification [8]. A total of 7.4×10^8 (6.7×10^8) events with γ-ray fold of three or higher was recorded in the self-supported- (backed-)target run, as well as any Microball pulse height and timing information correlated with the event trigger. The efficiencies for identifying protons and α particles were found to be about $\varepsilon_p \approx 65\%$ and $\varepsilon_\alpha \approx 50\%$, respectively. Events were selected off-line, in which exactly two α particles were detected; 1.4×10^7 (1.2×10^7) events satisfied this gating condition.

For each experiment, the 2α-gated events were unfolded into constituent twofold γ-γ coincidences and incremented into $E_\gamma(\text{all})-E_\gamma(\overline{\theta})$ matrices if at least one of the γ rays was detected by a Ge detector at specified angles θ. This γ-ray energy was included on the $E_\gamma(\overline{\theta})$ axis of the matrix. For the coincident γ ray, the energy of which was included on the E_γ(all) axis, any angle position was accepted. Those rings of Gammasphere with similar angles were combined in the same matrices: rings 2 and 3 ($\overline{\theta}=34.5°$), ring 4 (50.1°), rings 5 and 6 (66.5°), rings 7–11 (90°), rings 12 and 13 (114.0°), ring 14 (129.9°), and rings 15–17 (151.2°). The γ-ray energies on both axes were Doppler corrected using the average velocity β_{esc} measured for the recoils when escaping from the target. In addition, the measured α-particle energies and Microball detector angles were used to perform an event-by-event correction for the recoil ''kicks'' provided to the residual nucleus by the emitted α particles; this resulted in an improvement of about a factor of 3.5 in the measured γ-ray energy resolution. For the subsequent lifetime analysis, background-subtracted, angle-dependent spectra were projected from each matrix by gating on the E_γ(all) axes at energies corresponding to transitions within or decaying out of band 1 below the transitions of interest.

Residual Doppler shifts [9] were measured for transitions decaying out of the 16^+ through 6^+ states in band 1: For each transition, the γ-ray peak centroids were measured as a function of the angle $\overline{\theta}$ and used to extract the residual velocity $\langle\beta_{res}\rangle$ for the corresponding level. The residual and applied velocities, $\langle\beta_{res}\rangle$ and β_{esc}, were added, yielding the velocity $\langle\beta\rangle$. The latter was normalized to the maximum initial velocity β_0, defining the fractional velocity $\langle\beta\rangle/\beta_0$. The fractional velocities were corrected for a bias arising from gating with the Microball. Briefly put, the act of selecting events through charged-particle gating with an asymmetric-efficiency detector such as the Microball can create a biased data sample that has an average recoil velocity different from when the charged-particle detector was not used. (In the current example, the average velocity is reduced by about 15%.) This will be discussed in more detail separately [10].

The corrected fractional velocities are plotted in Figs. 2(a) and 2(b) for experiments 1 and 2a, respectively. It is preferable to gate above the transitions of interest when performing a lifetime analysis in order to avoid the influence of side feeding. However, the statistics are often not sufficient to do so. In the analysis of experiment 2a, it was possible to gate from above and measure centroid shifts for the 1880- and 2481-keV transitions [see Fig. 2(b)]. The value for the 1880-keV transition gated from above falls somewhat lower than the value obtained when gated from below, while the values for the 2481-keV transition agree within uncertainties. There is no indication of a significant systematic error arising from the side-feeding lifetimes.

To extract the Q_t values for these transitions, band 1 was modeled using a code developed by Lee [11]. Side feeding into each state was treated with the somewhat standard assumption that these transitions have the same lifetimes as the

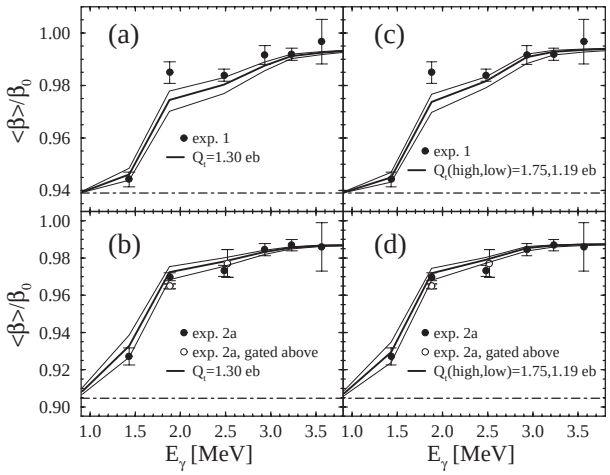

FIG. 2. Fractional recoil velocities for the transitions in band 1. Left: measured values (filled circles) for experiments (a) 1 and (b) $2a$ and calculated curves for $Q_t = 1.30 \pm 0.05 \pm 0.14$ e b. Right: measured values for experiments (c) 1 and (d) $2a$ and calculated curves for $Q_t(\text{high}) = 1.75^{+0.28}_{-0.30} \pm 0.21$ e b and $Q_t(\text{low}) = 1.19^{+0.06}_{-0.05} \pm 0.13$ e b. The open circles in (b) and (d) are the results obtained when gating above the transition. The data point for the 2481-keV transition has been offset in energy for clarity. The thin, solid lines in each panel indicate the statistical and systematic uncertainties, added in quadrature. The dot-dashed horizontal line in each panel marks the escaping recoil velocity.

in-band transitions feeding the states with the same spins. Intensities were taken from the experimental data. Stopping powers for the target materials were taken from Ref. [12]. The modeled $\langle\beta\rangle/\beta_0$ curve was compared with the data and χ^2 was minimized by adjusting the values of Q_t.

A significant change was made to the lifetime analysis of Ref. [1] regarding the treatment of parallel decay paths. As is seen in Fig. 1, there is extensive feeding from band 1 into band 2. The lifetime of a state with more than one decay branch is shorter than the partial lifetime for the in-band transition; thus, the modeled recoil velocity for a state that decays in part out of the band should be larger than if there was solely in-band decay. To take this into account in the analysis, the code of Ref. [11] was modified to allow a branching ratio B=(in band intensity)/(total intensity) to be entered as an input for each state. The partial lifetime for each in-band transition, determined through the value of Q_t, is then scaled by the branching ratio to yield the lifetime of the state, from which $\langle\beta\rangle/\beta_0$ is calculated. For states such as the $I^\pi = 8^+$ state in band 1 where $B \sim 20\%$, this effect is quite pronounced, leading to the elevated data point at 1880 keV seen in Fig. 2.

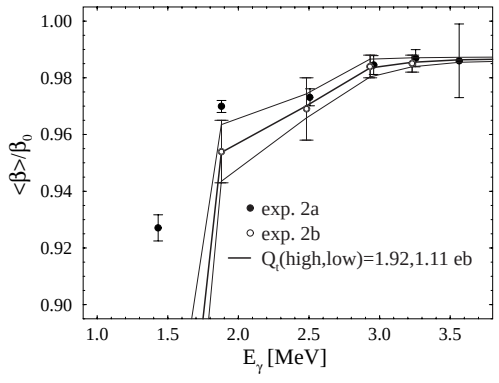

FIG. 3. Fractional recoil velocities for experiment 2b (open circles) in comparison with the corresponding best-fit values of $Q_t(\text{high}) = 1.92^{+2.10}_{-0.48} \pm 0.21$ e b and $Q_t(\text{low}) = 1.11^{+0.23}_{-0.14} \pm 0.13$ e b. The results from experiment $2a$ (filled circles) are also shown. The data point for the 2481-keV transition has been offset in energy for clarity. The thin lines indicate the statistical and systematic uncertainties, added in quadrature, on the values of Q_t. The escaping recoil velocity is off-scale, around $\langle\beta\rangle/\beta_0 = 0.45$.

As in Ref. [1], a constant Q_t value was initially assumed for all levels in band 1. The thin-target data, from experiments 1 and $2a$, were fitted in parallel using the same value of Q_t for each dataset, and the combined χ^2 was minimized. The best-fit value is $Q_t = 1.30 \pm 0.05 \pm 0.14$ e b, and is presented in Table I. The first uncertainties quoted are statistical and reflect the values of Q_t for which χ^2 increases by 1. The second uncertainties quoted are systematic and are estimated from the difference in value of Q_t when each experiment is fitted independently, including the uncertainties in the bias correction and in the stopping powers ($\sim 10\%$). The fractional velocity curves calculated for each experiment at the best-fit Q_t value are shown in panels (a) and (b) of Fig. 2.

The assumption of a constant Q_t throughout the entire band is probably simplistic. The aforementioned decay from band 1 to band 2 suggests that the configuration for band 1 at low spins may be admixed with that of band 2, and possibly others. The above fits were repeated, but using two separate Q_t values, Q_t(high) for the 2932-, 3230-, and 3563-keV transitions from the high-spin states, and Q_t(low) for the 1432-, 1880-, and 2481-keV transitions from lower-spin states in the band. Again, the combined χ^2 was minimized for this two-parameter fit, resulting in the best-fit values $Q_t(\text{high}) = 1.75^{+0.28}_{-0.30} \pm 0.21$ e b and $Q_t(\text{low}) = 1.19^{+0.06}_{-0.05} \pm 0.13$ e b (see Table I). The curves calculated at these Q_t values are presented in Figs. 2(c) and 2(d). Clearly, separating the fit into two values for Q_t reveals a considerably smaller result for the lower-spin states as compared to the high-spin states. The result of $Q_t = 1.30$ e b when a single ''average'' value is used reflects the greater sensitivity of the fit to the transitions on the falling part of the $\langle\beta\rangle/\beta_0$ curve; this is also apparent in the relative sizes of the uncertainties for the Q_t(high) and Q_t(low) moments.

The aim of the backed-target measurement of experiment $2b$ was to increase the sensitivity to the lifetimes of the lower-spin states. The Ta backing continues to reduce the recoil velocity of those nuclei that would have otherwise escaped from the target in experiment $2a$. This has the effect of stretching out the $\langle\beta\rangle/\beta_0$ curve to lower values. (Note that the backing in experiment $2b$ was not sufficient to bring the recoils to rest, but only to reduce the velocity to about $\langle\beta\rangle/\beta_0 = 0.45$.) The centroid shifts of the 1880-, 2481-, 2932-, and 3230-keV transitions in band 1 were measured in these backed-target data. It was not possible to obtain a meaningful fit for the 1432-keV transition in this dataset, in

TABLE I. Deduced Q_t values for the transitions in the SD band of ^{40}Ca. The first column gives the experiment(s) (see text). The notation $1Q_t$ or $2Q_t$ fit indicates that one or two average Q_t values were fitted to several transitions (residual Doppler shift analysis), while LS indicates a Doppler-broadened line-shape analysis. The remaining columns are headed by the transition energies in keV, and give the corresponding values of Q_t in e b. Only the statistical errors are listed here.

Expt.	Fit	1432	1880	2481	2932	3230	3563
Ref. [1]	$1Q_t$	$1.80^{+0.39}_{-0.29}$	$1.80^{+0.39}_{-0.29}$	$1.80^{+0.39}_{-0.29}$	$1.80^{+0.39}_{-0.29}$	$1.80^{+0.39}_{-0.29}$	$1.80^{+0.39}_{-0.29}$
$1+2a$	$1Q_t$	$1.30^{+0.05}_{-0.05}$	$1.30^{+0.05}_{-0.05}$	$1.30^{+0.05}_{-0.05}$	$1.30^{+0.05}_{-0.05}$	$1.30^{+0.05}_{-0.05}$	$1.30^{+0.05}_{-0.05}$
$1+2a$	$2Q_t$	$1.19^{+0.06}_{-0.05}$	$1.19^{+0.06}_{-0.05}$	$1.19^{+0.06}_{-0.05}$	$1.75^{+0.28}_{-0.30}$	$1.75^{+0.28}_{-0.30}$	$1.75^{+0.28}_{-0.30}$
$2b$	$2Q_t$		$1.11^{+0.23}_{-0.14}$	$1.11^{+0.23}_{-0.14}$	$1.92^{+2.10}_{-0.48}$	$1.92^{+2.10}_{-0.48}$	
$1+2a,b$	$2Q_t$	$1.18^{+0.06}_{-0.05}$	$1.18^{+0.06}_{-0.05}$	$1.18^{+0.06}_{-0.05}$	$1.81^{+0.41}_{-0.26}$	$1.81^{+0.41}_{-0.26}$	$1.81^{+0.41}_{-0.26}$
$2b$	LS		$1.01^{+0.09}_{-0.08}$	$1.53^{+0.14}_{-0.15}$	$1.46^{+0.48}_{-0.27}$		

part because there is some overlap between this transition and the 1374-keV $4_1^+ \rightarrow 2_1^+$ transition at backward angles. The fractional velocities for the fitted transitions were determined and are given as open circles in Fig. 3. The values deduced from experiment $2a$ are also shown on the plot as filled circles, for comparison. As expected, the average velocities are lower in experiment $2b$ than in $2a$, and the difference increases down the band. A two-parameter fit to these data results in the best-fit values $Q_t(\text{high}) = 1.92^{+2.10}_{-0.48} \pm 0.21$ e b and $Q_t(\text{low}) = 1.11^{+0.23}_{-0.14} \pm 0.13$ e b, also shown in Fig. 3. These results are consistent with those from experiments 1 and $2a$. Simultaneously fitting all three datasets results in the following values: $Q_t(\text{high}) = 1.81^{+0.41}_{-0.26} \pm 0.21$ e b and $Q_t(\text{low}) = 1.18^{+0.06}_{-0.05} \pm 0.13$ e b (see Table I). For a rigid, axially-symmetric rotor, these correspond to quadrupole deformations of $\beta_2(\text{high}) = 0.59^{+0.11}_{-0.07} \pm 0.06$ and $\beta_2(\text{low}) = 0.40 \pm 0.02 \pm 0.04$, thus confirming the superdeformed nature of the band. It should be noted that the Q_t moment deduced for the low-spin states is not inconsistent with the value of $Q_t = 1.69^{+0.42}_{-0.32}$ e b for the 914-keV transition given in Ref. [5].

The backed-target data provide the opportunity to perform a Doppler-broadened line-shape analysis. Spectra for this analysis were created in a fashion similar to those for the centroid shift analysis. Here, the energies incremented on the $E_\gamma(\overline{\theta})$ axis of the matrix had a zero applied recoil velocity and were, hence, recoil corrected but not Doppler corrected. Those energies on the E_γ(all) axis (the gating axis) were Doppler corrected in one set of matrices with $\beta = 0.02$, approximately the escaping recoil velocity, for gating on slower transitions, and $\beta = 0.042$ in another set of matrices for gating on faster transitions. The Gammasphere rings used in this analysis were grouped as follows: rings 2 and 3 combined, 9, and 15 and 16 combined formed one set of spectra, and rings 4, 9, and 14 formed a second set. Spectra were created for the 1880- and 2481-keV transitions by gates from both below and above the states of interest, and for the 2932- and 3230-keV transitions from gates below the states. In addition, spectra were created for the 2176-keV transition decaying out of the 8^+ state of band 1, parallel to the 1880-keV transition.

Lifetimes of each state were determined using the LINESHAPE analysis codes of Wells and Johnson [13], modified to handle input of the backing thickness so that in the simulations the recoils are not assumed to stop in the backing. These codes were used to generate 5000 Monte Carlo simulations of the velocity history of recoiling nuclei traversing the target and backing material in time steps of 0.001 ps. The number of time steps was limited to a maximum of 1000. Stopping powers were taken from the tabulations of Northcliffe and Schilling with corrections for atomic shell effects [14].

A detailed description of the line-shape fitting procedure can be found in, e.g., Ref. [15]. The intensities of the side-feeding transitions were taken from experiment $2a$ when fitting the spectra gated from below, or set to zero when gated from above. Each side-feeding cascade was treated as a sequence of three γ rays with an independent Q_t parameter and the same $\mathcal{J}^{(2)}$ moment of inertia as the average value for the in-band transitions. The three spectra from each set of rings were fitted simultaneously. Examples of these fits are given in Fig. 4. These peaks are not shifted much from their fully shifted energies, reflecting the short lifetimes of these states. Nevertheless, Q_t values could still be extracted from the line-shape fits. The weighted average Q_t for each state was determined from the results of the global fits to the sequences when gated from below and when gated from above, where applicable, as well as for the two parallel decay paths through the 2176- and 1880-keV transitions. (As discussed earlier, there is no clear systematic error evident when including the effects of side feeding.) The relevant branching ratios were again included in the determination of the Q_t moments. The resulting values for Q_t are $1.46^{+0.48}_{-0.27}$, $1.53^{+0.14}_{-0.15}$, and $1.01^{+0.09}_{-0.08}$ e b for the 2932-, 2481-, and 1880-keV transitions, respectively (see Table I). A meaningful Q_t value was not determined for the 3230-keV transition, as the deduced lifetime for this transition acted only as an effective feeding time for the levels below it.

These results, particularly for the line-shape analysis of the individual states, provide clear evidence that the Q_t values are smaller at lower spins in band 1. This is in contrast with the behavior of the highly collective band in ^{36}Ar. The lifetime analysis in Ref. [3] indicates that the $B(E2)$ (and, hence, Q_t) values in that band decrease with increasing spin, which has been attributed to a change in the nuclear shape towards oblate noncollectivity as the band approaches termi-

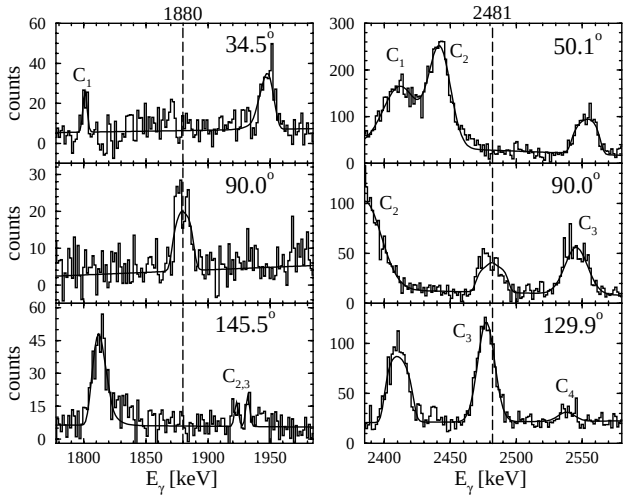

FIG. 4. Examples of line shapes from experiment 2*b*. The left panels show spectra for the 1880-keV peak, gated from above, in rings (top) 2 and 3, (middle) 9, and (bottom) 15 and 16. The right panels show spectra for the 2481-keV peak, gated from below, in rings (top) 4, (middle) 9, and (bottom) 14. The dashed lines mark the unshifted positions of the transitions. The C_i labels mark the positions of contaminant peaks. Note that since the recoils do not come to rest in the backing, even the slowest transitions exhibit Doppler shifts.

nation. This does not appear to be the case in ^{40}Ca, and is possibly due to the fact that the terminating state should be higher in this nucleus by several units of spin.

In several theoretical analyses, such as the relativistic mean field calculations discussed in Ref. [1], the fixed-configuration deformed Hartree-Fock calculations of Ref. [16], and the recent *sd-pf* shell model calculations of Ref. [17], quadrupole moments between 1.7 and 2.0 *e* b (quadrupole deformation $\beta_2 \sim 0.6$) have been consistently predicted for states in band 1. In Ref. [17], an attempt was also made to reproduce the properties of band 1 by including mixing of different *n*p-*n*h configurations. Components with $n>8$ were found to be absent, as these configurations lie too high in excitation energy. The predominant admixture with the 8p-8h configuration was found to be the 4p-4h configuration, which has less quadrupole collectivity and, hence, decreases the quadrupole moments in the band. Experimentally, the very large predicted Q_t moment is only observed at high spins, indicative of a rather pure 8p-8h nature. The decreased Q_t values at low spins deduced in the present work, however, are suggestive of configuration mixing, and place more stringent tests on calculations than the previous measurements in Ref. [1].

In summary, the quadrupole moments of several transitions within the SD band of ^{40}Ca were measured in a series of experiments. A smaller average Q_t than reported previously in Ref. [1] was determined when assuming a fixed value throughout the band, $Q_t = 1.30 \pm 0.05 \pm 0.14$ *e* b. On the other hand, separating the fit into two values of Q_t for the high- and low-spin states in the band results in the values $Q_t(\text{high}) = 1.81^{+0.41}_{-0.26} \pm 0.21$ *e* b and $Q_t(\text{low}) = 1.18^{+0.06}_{-0.05} \pm 0.13$ *e* b. This is consistent with an interpretation of band 1 as an SD band with a rather pure 8p-8h configuration at high spins, and an admixture of $n \leqslant 8$ *n*p-*n*h configurations at low spins. The detailed behavior of the variation of Q_t with spin, however, has not yet been reproduced by current theoretical efforts.

This work was supported in part by the U.S. Department of Energy, Nuclear Physics Division, under Grant No. DE-FG02-88ER-40406 and Contracts Nos. W-31-109-ENG-38 and DE-AC03-76SF00098, and by the Swedish Research Council.

[1] E. Ideguchi *et al.*, Phys. Rev. Lett. **87**, 222501 (2001).
[2] C.E. Svensson *et al.*, Phys. Rev. Lett. **85**, 2693 (2000).
[3] C.E. Svensson *et al.*, Phys. Rev. C **63**, 061301(R) (2001).
[4] D. Rudolph *et al.*, Phys. Rev. C **65**, 034305 (2002).
[5] J.L. Wood *et al.*, Phys. Rep. **215**, 101 (1992).
[6] W.J. Gerace and A.M. Green, Nucl. Phys. **A123**, 241 (1969).
[7] I.Y. Lee, Nucl. Phys. **A520**, 641c (1990).
[8] D.G. Sarantites *et al.*, Nucl. Instrum. Methods Phys. Res. A **381**, 418 (1996).
[9] B. Cederwall *et al.*, Nucl. Instrum. Methods Phys. Res. A **354**, 591 (1995).
[10] C.J. Chiara, D.R. LaFosse, D.G. Sarantites, M. Devlin, F. Lerma, and W. Reviol (unpublished).
[11] I.Y. Lee (private communication).
[12] J.F. Ziegler, *The Stopping and Ranges of Ions in Matter* (Pergamon, New York, 1980), Vol. 5.
[13] J.C. Wells and N.R. Johnson (private communication).
[14] L.C. Northcliffe and R.F. Schilling, Nucl. Data, Sect. A **7**, 233 (1970).
[15] C.J. Chiara *et al.*, Phys. Rev. C **64**, 054314 (2001).
[16] D.C. Zheng, L. Zamick, and D. Berdichevsky, Phys. Rev. C **42**, 1004 (1990).
[17] E. Caurier, F. Nowacki, A. Poves, and A. Zuker, nucl-th/0205036.